

**LiF-MgB<sub>2</sub> system for Reversible Hydrogen Storage**

Journal:	<i>The Journal of Physical Chemistry</i>
Manuscript ID:	Draft
Manuscript Type:	Article
Date Submitted by the Author:	
Complete List of Authors:	Gosalawit, Rapee; GKSS research center, Material Research Center Dornheim, Martin; Institute of Materials Research, Dept. of Nanotechnology von Colbe, José; Institute of Materials Research, Dept. of Nanotechnology Jensen, Torben; University of Aarhus, Interdisciplinary Nanoscience Center, Department of Chemistry Suarez, Karina; Institute of Materials Research, Dept. of Nanotechnology Bonatto, Christian; Institute of Materials Research, Dept. of Nanotechnology Peschke, Maik; Institute of Materials Research, Dept. of Nanotechnology Cerenius, Yngve; Lund University, Maxlab Bormann, Rüdiger; Universitätsverwaltung



**LiF–MgB<sub>2</sub> system for Reversible Hydrogen Storage**

R. Gosalawit<sup>1,\*</sup>, J. M. Bellosta von Colbe<sup>1</sup>, M. Dornheim<sup>1</sup>, T. R. Jensen<sup>2</sup>, Y. Cerenius<sup>3</sup>, K. Suarez<sup>1</sup>, Christian M. Bonatto<sup>1</sup>, Maik Peschke<sup>1</sup>, R. Bormann<sup>1</sup>

<sup>1</sup>Institute of Materials Research, GKSS Research Centre Geesthacht GmbH, D-21502 Geesthacht, Germany.

<sup>2</sup>Interdisciplinary Nanoscience Center (iNANO) and Department of Chemistry, University of Aarhus, Langelandsgade 140, DK-800 Aarhus C, Denmark.

<sup>3</sup>MaXLAB, Lund University, S-22100 Lund, Sweden.

**Abstract**

LiF–MgB<sub>2</sub> composites are proposed for reversible hydrogen storage. With respect to pure LiBH<sub>4</sub>, a significantly kinetic destabilization regarding hydrogenation and dehydrogenation is accomplished. The measured reversible hydrogen capacity amounts to 6.4 wt.%. The kinetic properties are improved significantly during cycling. The formation of a hydridofluoride phase (LiBH<sub>4-y</sub>F<sub>y</sub>) due to the fluorine anions substitution for hydrogen anions in [BH<sub>4</sub>]<sup>-</sup> is observed by synchrotron XRD and ATR-FTIR. Hydrogenation and dehydrogenation mechanisms are described based on the fluorine substitution in LiBH<sub>4</sub>.

\* Corresponding author

Keywords: Hydrogen storage material, Metal hydride, X-ray diffraction, Anion substitution, Synchrotron XRD

## 1. Introduction

Global warming as well as the inevitable exhaustion of petroleum reserves necessitates the development of alternative energy sources as well as novel energy carriers. Hydrogen utilised as an alternative carbon neutral energy carrier has become a significant contender in the mobile sector because of its abundance and environmentally benign oxidation product (water). Thus, high capacity reversible storage of hydrogen is one of the key challenges for fuel cell systems, especially in the automotive field. Solid-state metal hydrides have a potential to fulfill future hydrogen storage goals due to their definite advantages from the point of view of safety, compactness, and efficient storage as compared to the traditional high-pressure and liquid hydrogen storage systems [1-2]. Among them, the complex hydride  $\text{LiBH}_4$  is a potential candidate due to its high gravimetric and volumetric hydrogen density of 18.5 wt.% and  $121 \text{ kg/m}^3$ , respectively [1].  $\text{LiBH}_4$  can be decomposed into two steps:



By Eq. (1), 13.5 wt.% of hydrogen is desorbed to LiH and B only at temperatures above  $400 \text{ }^\circ\text{C}$ , while the further desorption (Eq. (2)) is not technically promising because of the requirement of very high temperature [3]. Moreover, Züttel et al. [4] reported the sluggish desorption kinetics of  $\text{LiBH}_4$ , i.e., half of the hydrogen in  $\text{LiBH}_4$  (9 wt.%) was released at temperatures up to  $600 \text{ }^\circ\text{C}$  and only 2 wt.% at below  $400 \text{ }^\circ\text{C}$ . Not only kinetic limitations for the desorption of  $\text{LiBH}_4$  exist, but also the absorption process is performed at high temperature and hydrogen pressure of  $600 \text{ }^\circ\text{C}$  and 350 bar, respectively [5-7]. Owing to these limitations, many researches have focused on the improvement of the thermodynamic and kinetic properties of  $\text{LiBH}_4$ . One approach is the incorporation of additives or catalysts, e.g., dehydrating temperature decreased to approximately 473 K when  $\text{SiO}_2$  was used as a catalyst [8] as well as Mg-doped  $\text{LiBH}_4$  showing a reduction in desorption temperature of 30 K [9]. The other is reactive hydride composites (RHCs) of  $\text{LiBH}_4$  and  $\text{MgH}_2$ , in which an exothermic formation of  $\text{MgB}_2$  during an endothermic desorption results in lower reaction enthalpy [10-11].

Recently, an alternative strategy to adjust thermodynamic properties and destabilize complex hydrides was investigated via substituting hydrogen by fluorine [5, 12-14]. Based on

1  
2  
3 similar atomic radii and the same valency of -1 in most compounds, several complex  
4 hydridofluorides of alkaline and alkaline-earth, for example,  $\text{KCaH}_{3-x}\text{F}_x$  [12],  $\text{NaAlH}_{4-x}\text{F}_x$  [13]  
5 and  $\text{NaMgH}_2\text{F}$  [14], were studied. Coupled experimental and theoretical investigations found  
6 that substitution of fluorine anions ( $\text{F}^-$ ) for hydrogen anions ( $\text{H}^-$ ) renders a favorable  
7 thermodynamic modification [5, 13, 15-16]. For example, Eigen et al. [13] theoretically  
8 calculated the decrease in overall heat of reaction to 35 kJ/mol for Na-Al-F-H system obtained  
9 from  $\text{F}^-$  substitution in  $\text{Na}_3\text{AlH}_6$  during absorption. In the report of Brinks et al. [5], the mixed  
10 hydride/fluoride system ( $\text{Na}_3\text{AlH}_{6-x}\text{F}_x$ ) was destabilized relative to pure hydride system  
11 ( $\text{Na}_3\text{AlH}_6$ ): both absorption and desorption isotherms of  $\text{Na}_3\text{AlH}_{6-x}\text{F}_x$  system are well above  
12 the plateau pressures of  $\text{Na}_3\text{AlH}_6$ . In the case of theoretical calculations, Yin et al. [16]  
13 reported that the reaction enthalpy decreased with the number of  $\text{F}^-$  substituted in  $\text{LiBH}_4$   
14 ( $\text{Li}_8\text{B}_8\text{H}_{32-x}\text{F}_x$  supercell). They also reported based on their theoretical calculation that the  $\text{F}^-$   
15 substitution was not only viable in  $\text{LiBH}_4$  ( $\text{Li}_8\text{B}_8\text{H}_{32-x}\text{F}_x$ ) but also in  $\text{LiH}$  ( $\text{Li}_8\text{H}_{8-x}\text{F}_x$ ).  
16  
17  
18  
19  
20  
21  
22  
23  
24  
25

26 In this study,  $\text{LiF-MgB}_2$  with fluorine substitution, prepared by hydrogenation of  $\text{LiF}$   
27 and  $\text{MgB}_2$ , is proposed to alter the stability of the complex hydride. By means of synchrotron  
28 radiation powder X-ray diffraction (SR-PXD) and fourier-transform infrared spectroscopy  
29 (FTIR), the formation of  $\text{LiBH}_{4-x}\text{F}_x$  complex hydridofluorides and absorption-desorption  
30 reaction mechanisms were observed. Absorption-desorption reversibility and cycle efficiency  
31 were evaluated in a Sievert-type apparatus.  
32  
33  
34  
35  
36  
37  
38

## 39 2. Experimental

40  $\text{LiF}$  (99.99+% purity) was purchased from Sigma Aldrich GmbH, Steinheim,  
41 Germany.  $\text{MgB}_2$  was bought from Alfa Aesar, Karlsruhe, Germany. The two powders  $\text{LiF}$  and  
42  $\text{MgB}_2$  in the molar ratio of 2:1 were milled for 5 h using a Spex 8000 M Mixer Mill placed in  
43 an argon filled glovebox. Stainless steel vials, 10 mm stainless steel balls and a ball-to-powder  
44 ratio (BPR) of 10:1 were used for milling. This milled  $\text{LiF-MgB}_2$  was denoted as **s1**. The  
45 powder **s1** was hydrogenated (390 °C under 60 bar  $\text{H}_2$ ) and denoted as **s2**. The powder **s2** was  
46 dehydrogenated (420 °C under 5 bar  $\text{H}_2$ ) and denoted as **s3**.  
47  
48  
49  
50  
51  
52

53 Differential scanning calorimetry (DSC) and thermo-gravimetric analysis (TGA) were  
54 performed simultaneously by a Netzsch STA 409 in an argon glovebox. The powder **s2** was  
55 heated from room temperature (20 °C) to 550 °C with the heating rate of 5 K/min under an  
56 argon flow of 150 ml/min. The concentration of  $\text{H}_2$ ,  $\text{HF}$ ,  $\text{B}_2\text{H}_6$ ,  $\text{Ar}$  and  $\text{H}_2\text{O}$  in the exhaust gas  
57 was continuously analyzed in a Hiden HPR-20 QIC mass spectrometer (MS).  
58  
59  
60

1  
2  
3 The powders **s1**, **s2** and **s3** were characterized by x-ray diffraction (XRD) using a  
4 Bruker axis with Cu K $\alpha$ 1 radiation ( $\lambda=1.5406 \text{ \AA}$ ). The diffraction patterns were collected in the  
5 range of  $10^\circ$  to  $70^\circ$  ( $2\theta$ ) in steps of  $0.05^\circ$ . The powder was protected from air and humidity by  
6 encapsulation with a polyimide film (capton foil)  
7  
8  
9

10 Absorption-desorption reversibility and cycle efficiency were investigated by a  
11 carefully calibrated Sievert's type apparatus from HERA, Quebec, Canada. The powder  
12 samples of about 150 mg were filled in a high pressure-temperature vessel as a sample holder  
13 under argon atmosphere.  
14  
15  
16

17 In situ synchrotron radiation powder X-ray diffraction (SR-PXD) was performed at the  
18 MAX II Synchrotron in Lund, Sweden, at beamline I711 in the research laboratory MAX-lab  
19 [17]. A Mar165 CCD detector was exposed 30 s with a selected X-ray wavelength of  
20  $1.09801 \text{ \AA}$  for each powder diffraction pattern. The samples were encapsulated airtight in  
21 sapphire capillaries in an argon glovebox. The heating was applied by the tungsten wire  
22 wrapped around the capillary while the temperature was controlled by the external PID  
23 regulator and thermocouple inserted into powder-bed as a schematic draw shown elsewhere  
24 [6]. The powders **s1** and **s2** were heated from room temperature ( $20^\circ\text{C}$ ) to  $390^\circ\text{C}$ , held at  $390^\circ\text{C}$   
25 for 2 h and cooled down to room temperature ( $20^\circ\text{C}$ ). Hydrogen pressure was maintained  
26 constantly during the experiments at 60 bar and 5 bar for hydrogenation and dehydrogenation,  
27 respectively.  
28  
29  
30  
31  
32  
33  
34  
35  
36

37 Fourier-transform infrared (FTIR) spectra were identified by an attenuated total  
38 reflection-FTIR (ATR-FTIR) spectroscopy using a Bruker Equinox 55. The sample powder  
39 was placed on an ATR sample holder over infrared radiation and covered by a tight screw.  
40 The spectra were collected in the wavenumber range of  $4000\text{-}550 \text{ cm}^{-1}$  with 64 scans for both  
41 sample and background.  
42  
43  
44  
45  
46  
47

### 48 **3. Results and discussion**

#### 49 **3.1. Reversible hydrogen storage**

50  
51 In order to confirm the ability of this LiF–MgB<sub>2</sub> system to absorb hydrogen as well as  
52 the determination of its hydrogenation temperature, the powder **s1** was subjected to a  
53 hydrogen pressure of 60 bar and continuously heated from room temperature ( $20^\circ\text{C}$ ) to  $400^\circ\text{C}$   
54 at the approximate rate of  $5 \text{ K/min}$ . Hydrogen absorption started slowly at around  $370^\circ\text{C}$   
55 and increased gradually up to the temperature of  $390^\circ\text{C}$ . Therefore, the suitable condition for  
56 hydrogenation of this LiF–MgB<sub>2</sub> mixture was at  $390^\circ\text{C}$  and 60 bar hydrogen.  
57  
58  
59  
60

1  
2  
3 After hydrogenation for 20 h, the dehydrogenation behavior of **s2** was evaluated by  
4 simultaneous TGA, DSC and MS measurements. The DSC thermogram shows three  
5 endothermic peaks (Fig. 1). The first two endothermic peaks in the temperature ranges of 112  
6 to 130 °C and 262 to 280 °C refer to the transformation from orthorhombic to hexagonal  
7  $\text{LiBH}_4$  and melting of hexagonal  $\text{LiBH}_4$ , respectively, while the third one at around 420-490  
8 °C indicates the dehydrogenation of  $\text{LiBH}_4$  [6, 18]. Therefore, the desorption temperature  
9 used for this  $\text{LiF-MgB}_2$  system based on the decomposition temperature of  $\text{LiBH}_4$  (DSC  
10 thermogram) was 420 °C. The TGA and MS results show a significant weight loss of about  
11 4.6 wt.% and the hydrogen signal, respectively, corresponding to the dehydrogenation  
12 observed by DSC (Fig. 1). One of the most important concerns for this borohydride/fluoride  
13 hydrogen storage system is the formations of hydrofluoric acid (HF) and diborane ( $\text{B}_2\text{H}_6$ )  
14 during dehydrogenation. This could cause corrosion on various fuel cell components and  
15 unrecoverable boron loss, respectively [5, 13]. However, by MS measurements, hydrofluoric  
16 acid and diborane are not detected in the exhaust gas during dehydrogenation of **s2** (Fig. 2).  
17  
18  
19  
20  
21  
22  
23  
24  
25  
26  
27

28 The investigation of phases formed during hydrogenation and dehydrogenation was  
29 done by XRD. Fig. 3 shows the specific diffraction peaks of  $\text{MgB}_2$  and  $\text{LiF}$  in **s1** as expected.  
30 After hydrogenation, the characteristic peaks of  $\text{LiBH}_4$  and  $\text{MgF}_2$  are observed together with  
31 those of residual  $\text{LiF}$  and  $\text{MgB}_2$  (Fig. 3). This implies successful hydrogenation of this  
32  $\text{LiF-MgB}_2$  system to obtain  $\text{LiBH}_4$ . Thereafter, the hydrogen desorption of **s2** was performed  
33 at 420 °C under 5 bar  $\text{H}_2$  for several hours (~ 70 h). The powder **s3** shows the diffraction  
34 peaks of  $\text{LiF}$  and  $\text{MgB}_2$  as well as kinetically delayed behavior, which is revealed as partially  
35 unconverted  $\text{MgF}_2$  (Fig. 3). Although  $\text{MgF}_2$  was not completely converted to  $\text{MgB}_2$  and  $\text{LiF}$   
36 after dehydrogenation, the XRD intensity peak ratio of  $\text{MgB}_2$  (or  $\text{LiF}$ ) to  $\text{MgF}_2$  is increased  
37 after dehydrogenation compared to **s2**. This suggests a reversible reaction.  
38  
39  
40  
41  
42  
43  
44  
45  
46  
47

### 48 3.2. Hydrogenation, dehydrogenation and cycle efficiency

49 Hydrogenation, dehydrogenation and cycle efficiency of the  $\text{LiF-MgB}_2$  system were  
50 observed in more detail by a Sievert-type apparatus. Fig. 4 shows the first absorption for 20 h  
51 with a hydrogen capacity of ~ 6.6 wt. % while those of the second and the third cycles after 17  
52 h are ~ 5.6 wt.% and 6.0 wt.%, respectively. It should be noted that the second and the third  
53 cycles are significantly faster than the first cycle, e.g., at 4 h the second and the third cycles  
54 absorb hydrogen for 4.1 wt.% and 4.3 wt.%, respectively, while the first one is 0.9 wt.% (Fig.  
55 4). This indicates the kinetic improvement of the system in terms of absorption after cycling.  
56  
57  
58  
59  
60

1  
2  
3  
4  
5  
6  
7  
8  
9  
10  
11  
12  
13  
14  
15  
16  
17  
18  
19  
20  
21  
22  
23  
24  
25  
26  
27  
28  
29  
30  
31  
32  
33  
34  
35  
36  
37  
38  
39  
40  
41  
42  
43  
44  
45  
46  
47  
48  
49  
50  
51  
52  
53  
54  
55  
56  
57  
58  
59  
60

In the case of desorption, the first sluggish cycle is completed after 70 h with the hydrogen capacity of 6.4 wt.% while those of the second and third cycles are 5.6 wt.% (19 h) and 5.9 wt.% (12 h, 30 min), respectively (Fig. 5). This is relevant to the hydrogen capacity absorbed in each cycle as discussed previously. Moreover, the significantly kinetic improvement for desorption is achieved by cycling, i.e. at hydrogen capacity of 4 wt. %, the first cycle spends 21 h while those of second and third cycles are 11 h and 7 h, respectively (Fig. 5). The absorbed and desorbed hydrogen capacities detected from the second and the third cycles are inferior with respect to the first cycle. This might be explained by kinetic delay of partially unconverted  $\text{MgF}_2$  after first dehydrogenation as mentioned in section 3.1 resulting in the deficient amounts of  $\text{LiF}$  and  $\text{MgB}_2$  for the next cycles. However, it should be noted that the hydrogen capacities of hydrogenation and dehydrogenation in the second and the third cycles are equivalent. This implies that the partially unconverted  $\text{MgF}_2$  doesn't have any further influences to the cycle efficiency after the first cycle. In addition, compared to the highly kinetically limited  $\text{LiBH}_4$ , in which the hydrogenation and dehydrogenation succeed only at high temperature and hydrogen pressure, for example 600 °C and 350 bar for hydrogenation [5-7], this mixed  $\text{LiF-MgB}_2$  system is significantly destabilized.

Moreover, it should be noted that on one hand three different regimes of dehydrogenation are observed in the first dehydrogenation (Fig. 5) at 0-1 wt.%, 1-4.4 wt.% and 4.4-6.3 wt.% hydrogen capacity and on the other hand that the weight loss (wt. %) referring to hydrogen desorption (~4.6 wt. %) from TGA thermogram (section 3.1) is significantly less than the dehydrogenation achieved from desorption isotherm (6.4 wt. %). In the case of second and third dehydrogenation, a significant regime of hydrogen release is observed. Since the evidences from XRD and simultaneous TGA, DSC and MS cannot fulfill the explanation for these phenomena, SR-PXD measurement and ATR-FTIR were carried out.

### 3.3. Hydrogen absorption and desorption mechanisms

In order to describe the reaction mechanisms of hydrogen absorption and desorption of this mixed  $\text{LiF-MgB}_2$  system, SR-PXD and ATR-FTIR were carried out. From Fig. 6, the reflections corresponding to  $\text{MgF}_2$  start to be visible at about 316 °C and their intensity increases with temperature whereas the reflection intensities of  $\text{LiF}$  and  $\text{MgB}_2$  decrease. This indicates the proceeding of reaction during hydrogenation of milled  $\text{LiF-MgB}_2$  mixture.  $\text{LiBH}_4$  might be generated at the same time as  $\text{MgF}_2$  but the reflections do not appear because of its molten state. However,  $\text{LiBH}_4$  shows the reflections referring to hexagonal and orthorhombic phases at about 270-277 °C and 110-120 °C, respectively, during the cooling

1  
2  
3 state relevant to DSC thermogram (section 3.1 and Fig. 1). Moreover, a significant peak shift  
4 of LiF reflections at around 380 °C in both heating and cooling states are observed. This hints  
5 at the formation of  $\text{LiH}_{1-x}\text{F}_x$  as in previous observations for the NaF–Al system reported by  
6 Eigen et al. [13].  
7  
8  
9

10 For desorption, the sample **s2** from Sievert's type apparatus was investigated. Fig. 7  
11 shows the reflections for both hexagonal and orthorhombic phases of  $\text{LiBH}_4$  at temperatures  
12 relevant to those from the hydrogenation step (Fig. 6) and DSC thermogram (Fig. 1).  
13 Moreover, it should be noted that some parallel reflections to both phases of  $\text{LiBH}_4$  in the  
14 same temperature region are observed (Fig. 7). This might be assumed to be due to the  
15 formation of a single phase  $\text{LiBH}_{4-y}\text{F}_y$ . This suggests that the hydrogen anions ( $\text{H}^-$ ) might be  
16 substituted by fluorine anions ( $\text{F}^-$ ) in the  $\text{LiBH}_4$  phase during hydrogenation. These parallel  
17 phases of  $\text{LiBH}_{4-y}\text{F}_y$  to those of pure  $\text{LiBH}_4$ , which are appeared at the same temperature  
18 range, might be due to the similarities of  $\text{F}^-$  and  $\text{H}^-$ . In order to clarify the  $\text{F}^-$  ion substitution in  
19  $\text{LiBH}_4$ , the XRD spectra from SR-PXD measurements were intensively evaluated by  
20 PowderCell 2.4 program. The first and last spectra of absorption process from SR-PXD  
21 measurement, which belong to **s1** and **s2**, respectively, were chosen. Fig. 8 (a) reveals the  
22 corresponding spectra of LiF (cell volume of  $66.43 \text{ \AA}^3$ ) and  $\text{MgB}_2$ . In the case of **s2**,  $\text{LiBH}_4$ ,  
23  $\text{LiBH}_3\text{F}$ ,  $\text{MgF}_2$ ,  $\text{MgB}_2$  and LiF (cell volume of  $65.31 \text{ \AA}^3$ ) are observed (Fig. 8 (b)). It was  
24 found out that the  $\text{LiBH}_3\text{F}$  phase located adjacently to those of  $\text{LiBH}_4$ . Moreover, it should be  
25 noted that the cell volume of LiF is decreased after absorption. This might refer to the  
26 hydrogen substitution into LiF phase to obtain  $\text{LiH}_{1-x}\text{F}_x$  phase. This is relevant to the  
27 significant peak shift of LiF reflections at  $\sim 380 \text{ }^\circ\text{C}$  (SR-PXD spectra) during hydrogenation,  
28 which hints to the formation of  $\text{LiH}_{1-x}\text{F}_x$ .  
29  
30  
31  
32  
33  
34  
35  
36  
37  
38  
39  
40  
41  
42  
43

44 In order to reliably confirm the formation of  $\text{LiBH}_{4-y}\text{F}_y$  ( $\text{LiBH}_3\text{F}$ ), ATR-FTIR was  
45 performed. Fig. 9 shows the characteristic peaks of the commercial  $\text{LiBH}_4$ , i.e.,  $[\text{BH}_4]^-$   
46 stretching at 2300, 2274 and  $2180 \text{ cm}^{-1}$  and  $[\text{BH}_4]^-$  bending at 1311, 1287, 1239 and  $1091 \text{ cm}^{-1}$   
47 [19]. The powder **s2** reveals B-F stretching ( $1140 \text{ cm}^{-1}$ ) and bending ( $790$  and  $636 \text{ cm}^{-1}$ ) of  
48  $[\text{H}_{4-y}\text{B-F}_y]^-$  with most other peaks similar to  $\text{LiBH}_4$  (Fig. 9). This implies the substitution of  
49  $\text{F}^-$  for  $\text{H}^-$  in  $\text{LiBH}_4$  to form  $\text{LiBH}_3\text{F}$  during hydrogenation. The significantly shifted  
50 wavenumber of the B-F stretching vibration in  $[\text{H}_3\text{-B-F}]^-$  ( $1140 \text{ cm}^{-1}$ ) with respect to that in  
51 the case of  $[\text{BF}_4]^-$  ( $1044 \text{ cm}^{-1}$ ) [20] might be explained by the electronegativity effect. The  
52 lower electronegativity value compared to fluorine of the hydrogen, adjacent atom to B-F  
53 bond of  $[\text{H}_3\text{-B-F}]^-$ , enhances the single-bond character of B-F bond and causes infrared  
54 reflectance at higher wavenumbers. In addition, all powders show the characteristic peaks of  
55  
56  
57  
58  
59  
60

OH stretching ( $3461$  and  $3437\text{ cm}^{-1}$ ) and H-O-H bending ( $1635\text{ cm}^{-1}$ ) of water molecules. This might be due to the atmospheric humidity during the ATR-FTIR experiments. Moreover, due to the three different steps of hydrogen desorption at 0-1 wt.%, 1-4.4 wt.% and 4.4-6.3 wt.% (Fig. 5), further investigation was carried out to explain the reaction mechanisms. The ATR-FTIR spectrum of the powder **s2** after 1 wt. % dehydrogenation shows the characteristic peaks of  $[\text{BH}_4]^-$  and B-F (bending), while that of B-F (stretching) bond from  $[\text{H}_3\text{-B-F}]^+$  phase ( $1140\text{ cm}^{-1}$ ) has disappeared (Fig. 8). This indicates that the phase dehydrogenated for about 1 wt.% is a part of  $\text{LiBH}_{4-y}\text{F}_y$  with  $y < 2$  ( $\text{LiBH}_3\text{F}$ ) [13]. Thereafter, the powder **s2** continuously decomposed until 4.4 wt.% (the second dehydrogenation step). This might be related to the dehydrogenation of  $\text{LiBH}_4$  because it approaches to the hydrogen weight loss (%) from the TGA thermogram referring to the decomposition of  $\text{LiBH}_4$  (Fig. 1). Therefore, in the first and second hydrogen desorption steps, the dehydrogenation of  $\text{LiBH}_3\text{F}$  and  $\text{LiBH}_4$  were taking place, respectively.

Owing to the discussion and explanation for the system of  $\text{NaF-Al}$  [13], a part of  $\text{LiBH}_{4-y}\text{F}_y$  with  $y < 2$  ( $\text{LiBH}_3\text{F}$ ) might decompose at the first step (0-1 wt.%) and leave  $\text{LiBH}_{4-y}\text{F}_y$  with excessive fluorine ( $y > 2$ ). Together with the formation of  $\text{LiH}_{1-x}\text{F}_x$  during hydrogenation as shown in previous observations,  $\text{LiBH}_{4-y}\text{F}_y$  with excessive fluorine ( $y > 2$ ) can dehydrogenate only at highly endothermic reactions. Therefore, the slow kinetic during dehydrogenation of the last step (4.4-6.3 wt.%) might be obtained from the exchange of hydrogen anions from  $\text{LiH}_{1-x}\text{F}_x$  and fluorine anions from  $\text{LiBH}_{4-y}\text{F}_y$  ( $y > 2$ ) [13].

#### 4. Conclusions

The system of  $\text{LiF-MgB}_2$  was evaluated for reversible hydrogen storage. A significant destabilization for both hydrogenation and dehydrogenation of this system relative to highly stable  $\text{LiBH}_4$  was obtained. However, kinetic delay revealed as partially unconverted  $\text{MgF}_2$  after dehydrogenation in the first cycle caused an inferior hydrogen capacity in the second and the third cycles. From SR-PXD and ATR-FTIR results, the reaction mechanisms of hydrogenation and dehydrogenation in this  $\text{LiF-MgB}_2$  system were investigated. The substitution of fluoride anions ( $\text{F}^-$ ) in  $\text{LiBH}_4$  and that of hydrogen anions ( $\text{H}^-$ ) in  $\text{LiF}$  to achieve  $\text{LiBH}_{4-y}\text{F}_y$  ( $\text{LiBH}_3\text{F}$ ) and  $\text{LiH}_{1-x}\text{F}_x$ , respectively, were observed during hydrogenation. For dehydrogenation, three different decomposition steps were clarified as (i) dehydrogenation of  $\text{LiBH}_{4-y}\text{F}_y$  ( $y < 2$ ) ( $\text{LiBH}_3\text{F}$ ) ( $\sim 1$  wt.%); (ii) dehydrogenation of  $\text{LiBH}_4$

1  
2  
3 (~3.4 wt.%); and (ii) anion exchange between  $F^-$  and  $H^-$  of  $LiBH_{4-y}F_y$  ( $y>2$ ) and  $LiH_{1-x}F_x$  (~1.9  
4 wt.%).  
5  
6  
7

## 8 **Acknowledgement**

9  
10  
11  
12 The authors appreciate the financial support from the European Community in the  
13 frame of integrated project “NESSHY-Novel Efficient Solid State for Hydrogen Storage”  
14 (contract SES6-2006-518271). We also would like to acknowledge Dr. Peter Simon and Dr.  
15 Mauricio Schieda for helping in ATR-FTIR measurements.  
16  
17  
18  
19  
20  
21  
22  
23  
24  
25  
26  
27  
28  
29  
30  
31  
32  
33  
34  
35  
36  
37  
38  
39  
40  
41  
42  
43  
44  
45  
46  
47  
48  
49  
50  
51  
52  
53  
54  
55  
56  
57  
58  
59  
60

**References**

- [1] L. Schlapbach, A. Züttel, *Nature* 414 (2001) 353.
- [2] B. Sakintuna, F. L.-Darkrim, M. Hirscher, *Int. J. Hydrogen Energ.* 32 (2007) 1121.
- [3] M. Au, A. R. Jurgensen, W. A. Spencer, D. L. Anton, F. E. Pinkerton, S.-J. Hwang, C. Kim, R. C. Bowman Jr. II, *J. Phys. Chem. C* 112 (2008) 18661.
- [4] A. Züttel, S. Rentsch, P. Fischer, P. Wenger, P. Sudan, Ph. Mauron, Ch. Emmenegger, *J. Alloys Compd.* 356-357 (2003) 515.
- [5] H. W. Brinks, A. Fossdal, B. C. Hauback, *J. Phys. Chem. C* 112 (2008) 5658.
- [6] U. Bösenberg, S. Doppiu, L. Mosegaard, G. Barkhordarian, N. Eigen, A. Borgschulte, T. R. Jensen, Y. Cerenius, O. Gutfleisch, T. Klassen, M. Dornheim, R. Bormann, *Acta Mater.* 55 (2007) 3951.
- [7] P. Mauron, F. Buchter, O. Friedrichs, A. Remhof, M. Biemann, C.N. Zwicky, A. Züttel, *J. Phys. Chem. B* 112 (2008) 906
- [8] A. Züttel, S. Rentsch, P. Fischer, P. Wenger, P. Sudan, Ph. Mauron, *J. Alloys Compd.* 356-357 (2003) 515.
- [9] S. Orimo, Y. Nakamori, G. Kitahara, K. Miwa, N. Ohba, S. Towata, A. Züttel, *J. Alloys Compd.* 404-406 (2005) 427.
- [10] G. Barkhordarian, T. Klassen, M. Dornheim, R. Bormann, *J. Alloys Compd.* 440 (2007) L18.
- [11] M. Dornheim, S. Doppiu, G. Barkhordarian, U. Boesenberg, T. Klassen, O. Gutfleisch, R. Bormann, *Scr. Mater.* 56 (2007) 841.
- [12] J.-P. Soulié, J.-P. Laval, A. Bouamrane, *Solid State Sci.* 5 (2003) 273.
- [13] N. Eigen, U. Bösenberg, J. Bellosta von Colbe, T. R. Jensen, Y. Cerenius, M. Dornheim, T. Klassen, R. Bormann, *J. Alloys Compd.* 477 (2009) 76–80.
- [14] A. Bouamrane, J. P. Laval, J.-P. Soulié, J. P. Bastide, *Mater. Res. Bull.* 35 (2000) 545.
- [15] L.-C. Yin, P. Wang, X.-D. Kang, C.-H. Sun, H.-M. Cheng, *Phys. Chem. Chem. Phys.* 9 (2007) 1499.
- [16] L. Yin, P. Wang, Z. Fang, H. Cheng, *Chem. Phys. Lett.* 450 (2008) 318.
- [17] Y. Cerenius, K. Ståhl, L. A. Svésson, T. Ursby, Å Oskarsson, J. Albertsson, *J. Synchrotron Rad* 7 (2000) 203.

1  
2  
3 [18] L. Mosegaard, B. Møller, J.-E. Jørgensen, U. Bösenberg, M. Dornheim, J. C. Hanson, Y.  
4 Cerenius, G. Walker, H. J. Jakobsen, F. Besenbacher, T. R. Jensen, *J. Alloys Compd.*  
5 446-447 (2007) 301.  
6  
7

8  
9 [19] K. B. Harvey, N. R. McQuaker, *Can. J. Chemistry* 49 (1971) 3282.  
10

11 [20] S.-W. Song, T. J. Richardson, G. V. Zhuang, T. M. Devine, J. W. Evans, *Electrochim.*  
12 *Acta* 49 (2004) 1483.  
13  
14  
15  
16  
17  
18  
19  
20  
21  
22  
23  
24  
25  
26  
27  
28  
29  
30  
31  
32  
33  
34  
35  
36  
37  
38  
39  
40  
41  
42  
43  
44  
45  
46  
47  
48  
49  
50  
51  
52  
53  
54  
55  
56  
57  
58  
59  
60

1  
2  
3 Figure captions  
4  
5

6 Fig. 1. Simultaneous TGA, DSC and MS measurement of **s2**.  
7

8  
9 Fig.2. MS Spectra of **s2**.  
10

11 Fig. 3. XRD diffraction patterns of **s1**, **s2** and **s3**.  
12

13  
14 Fig. 4. Hydrogenation isotherm and cycling efficiency of **s1** at 390 °C under 60 bar H<sub>2</sub>.  
15

16  
17 Fig. 5. Dehydrogenation isotherm and cycling efficiency of **s2** at 420 °C under 5 bar H<sub>2</sub>.  
18

19  
20 Fig. 6. SR-PXD reflections of **s1** under 60 bar H<sub>2</sub> with the temperature program of (i) heating  
21 from 25-390 °C; (ii) isothermal condition at 390 °C for 2 h; and (iii) cooling down to 25 °C,  
22 low (●) and high (○) temperature phases of LiBH<sub>4-y</sub>F<sub>y</sub>.  
23  
24  
25

26 Fig. 7. SR-PXD reflections of **s2** under 5 bar H<sub>2</sub> with the temperature program of (i) heating  
27 from 25-390 °C; and (ii) isothermal condition at 390 °C for 2 h.  
28  
29

30  
31 Fig. 8. SR-PXD reflections (first frame) of **s1** (a) and **s2** (b) evaluated by PowderCell 2.4.  
32

33  
34 Fig. 9. ATR-FTIR spectra of LiBH<sub>4</sub>, **s2** and after 1 wt.% dehydrogenation of **s2**.  
35  
36  
37  
38  
39  
40  
41  
42  
43  
44  
45  
46  
47  
48  
49  
50  
51  
52  
53  
54  
55  
56  
57  
58  
59  
60

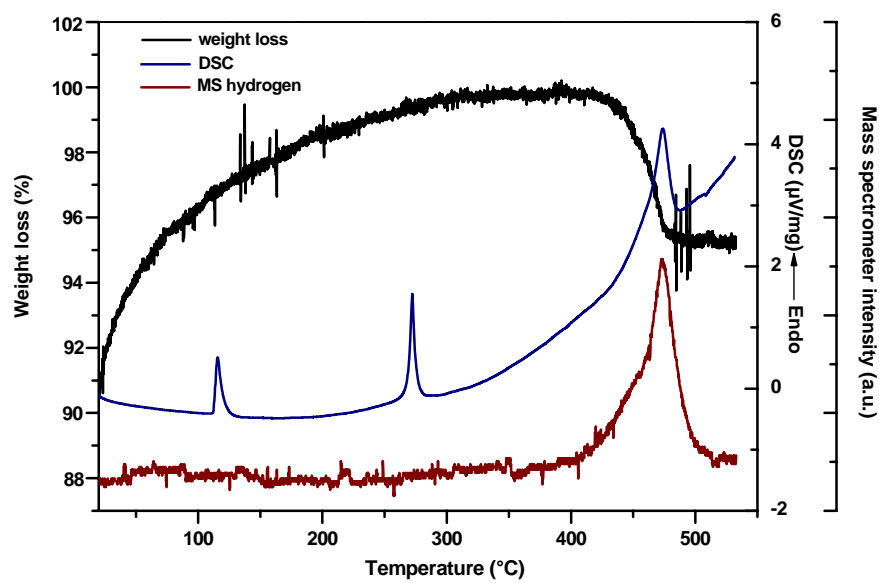


Fig. 1

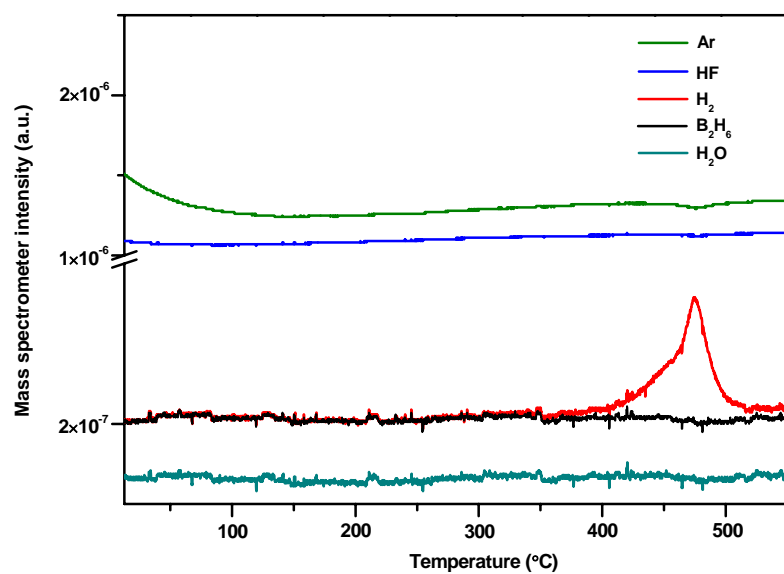


Fig. 2

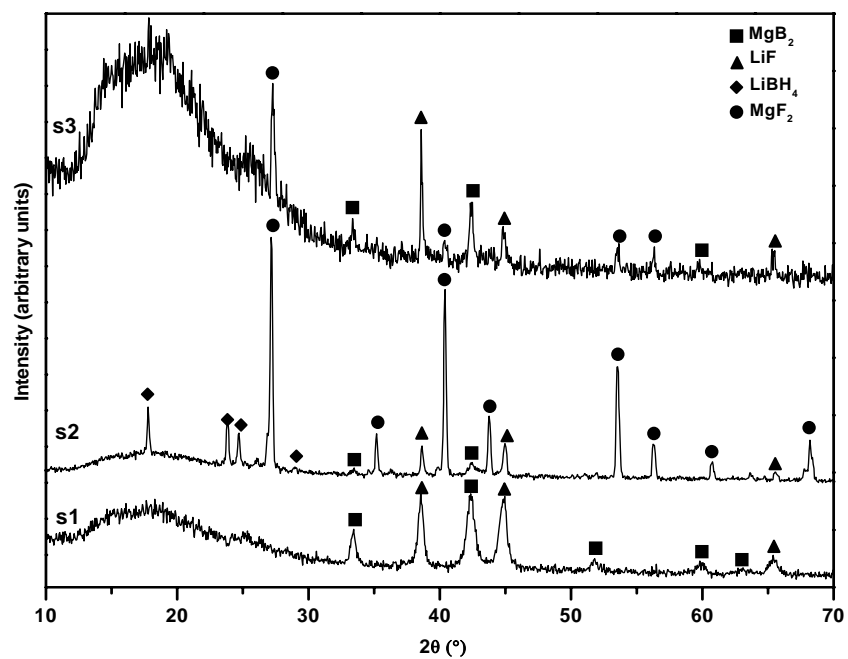


Fig. 3

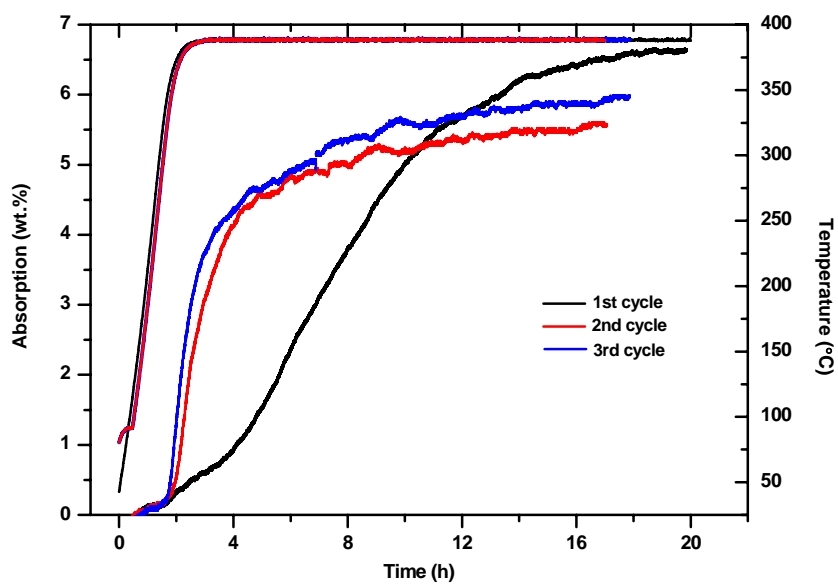


Fig. 4

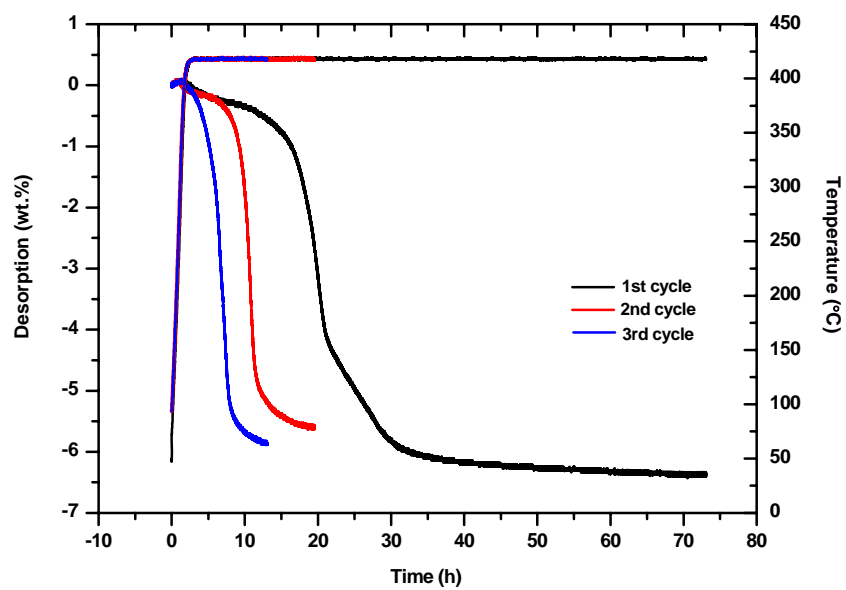


Fig. 5

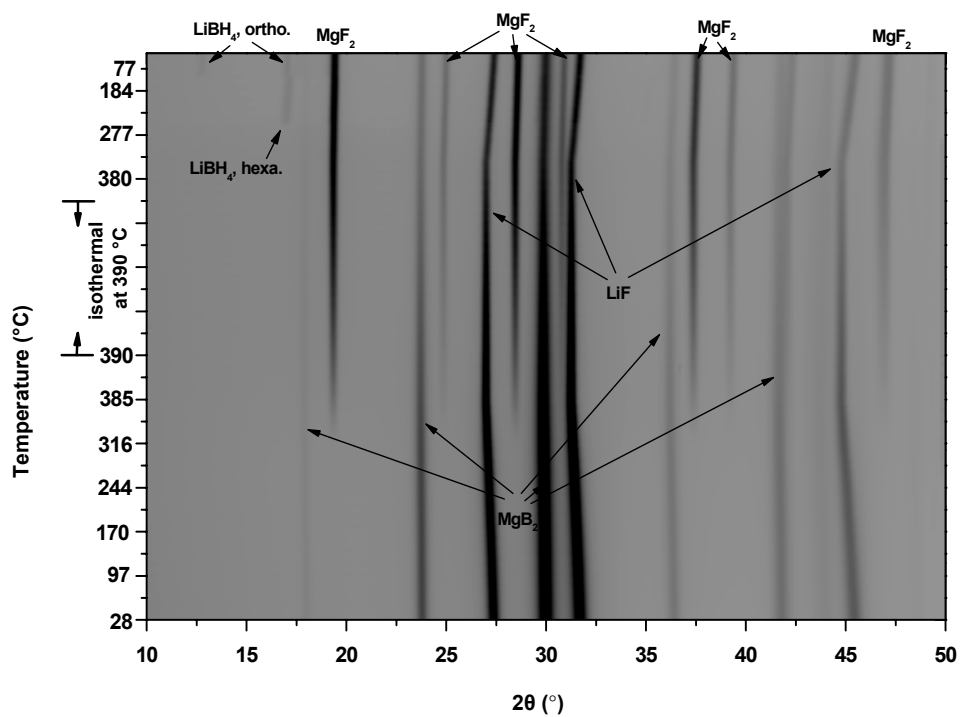


Fig. 6

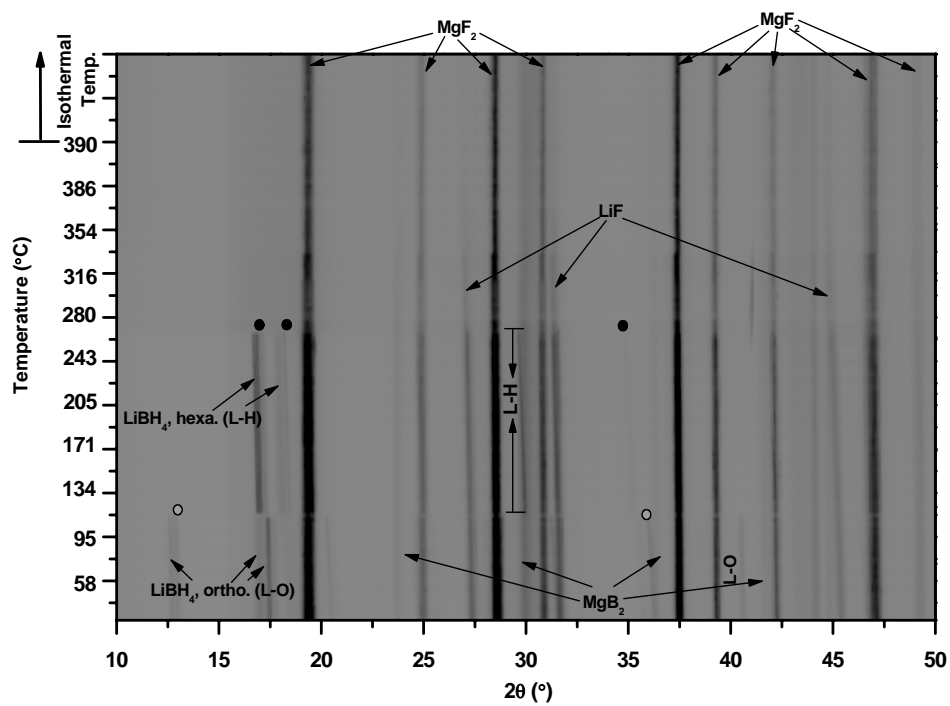
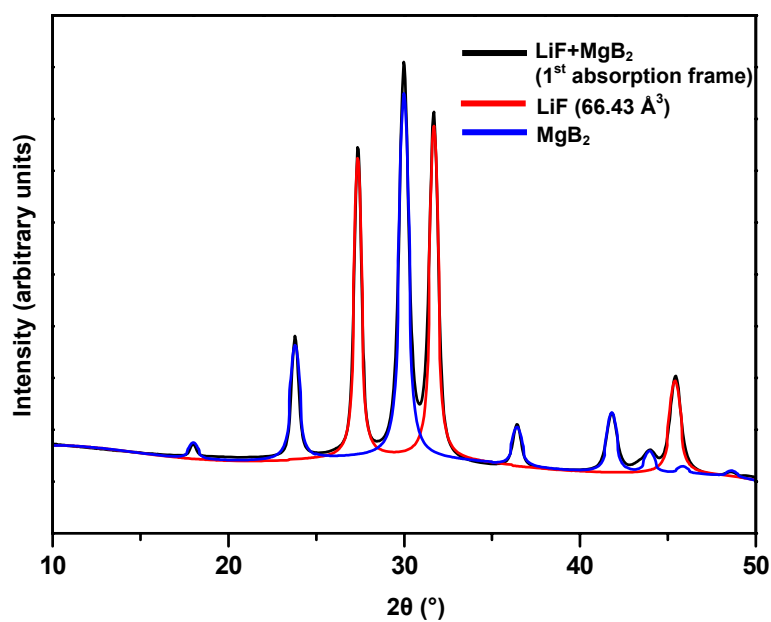
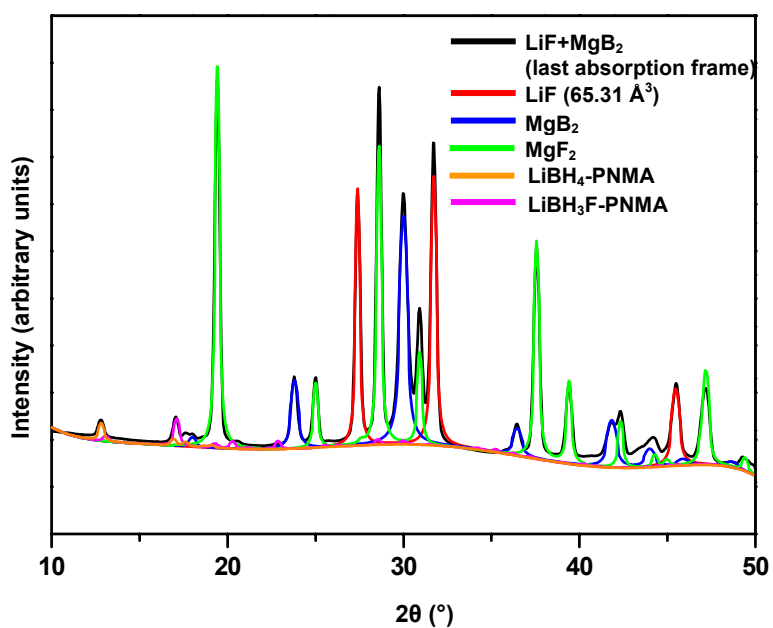


Fig. 7



(a)



(b)

Fig.8

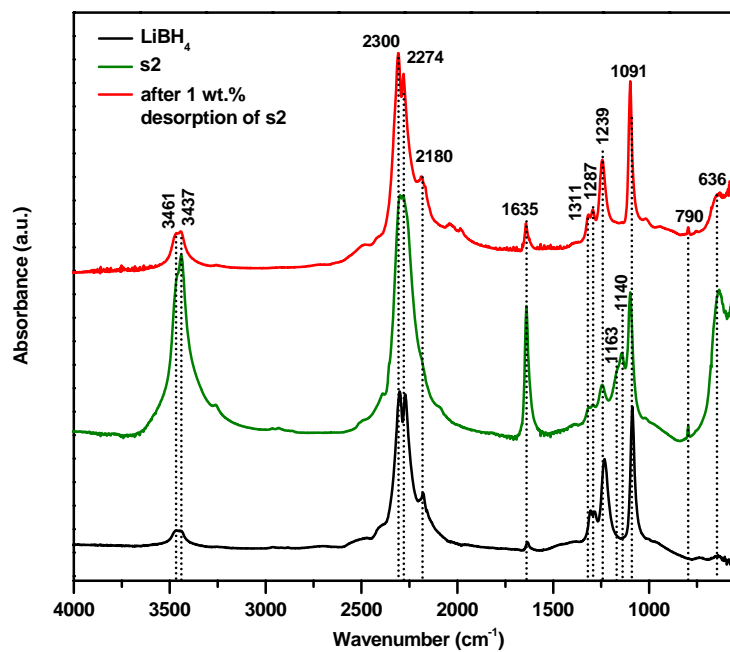


Fig. 9